Influence of snow surface properties on L-band brightness temperature at Dome C, Antarctica

Marion Leduc-Leballeur, G. Picard, G. Macelloni, L. Arnaud, M. Brogioni, A. Mialon, Y.H. Kerr

Influence of snow surface properties on L-band brightness temperature at Dome C, Antarctica

M. Leduc-Leballeur[a,b,*], G. Picard[b], G. Macelloni[a], L. Arnaud[b], M. Brogioni[a], A. Mialon[c], Y. H. Kerr[c]

[a] *IFAC—CNR, 50019 Sesto Fiorentino, Italy*
[b] *Univ. Grenoble Alpes, CNRS, IRD, Grenoble INP[1], IGE, F-38000 Grenoble, France*
[c] *CESBIO (CNES, CNRS, IRD, UPS), Univ. Toulouse, F-31401 Toulouse Cedex 09, France*

Abstract

L-band radiometer measurements collected over the Dome C area from 2010 to 2015 indicated that the brightness temperature (T_B) was relatively stable at vertical (V) polarization (standard deviation lower than 1 K at annual scale), while it was slightly more variable at horizontal (H) polarization. During the 2014-2015 austral summer, an exceptional situation was recorded by both the DOMEX ground radiometer and the European Space Agency (ESA)'s Soil Moisture and Ocean Salinity (SMOS) satellite. From November 2014 to March 2015, T_B H showed a progressive and significant increase until 20 March 2015 when it sharply decreased by about 5 K (at 52.5° incidence angle) within a few days. In parallel to the increase in T_B H, glaciological and meteorological in situ measurements showed a wind speed that was lower than usual and a low-density snow layer being progressively set up on the surface. This was consistent with the exceptional hoar event observed, as well as with snow accumulation on the surface. On the other hand, the decrease in T_B H was related to the passing over Dome C of a storm that removed or compacted the layer of light snow on the surface. The WALOMIS (Wave Approach for LOw-frequency MIcrowave emission in Snow) snow-emission model was used with in situ measurements of the snowpack as inputs for evaluating the effect of changes observed on the snow surface in T_B H. The simulations indicated that the surface snow density variations were sufficient for predicting the increasing and decreasing trends of the T_B H. However, the thickness variations of the superficial layer were essential so as to obtain a better agreement with the SMOS observations. This result confirmed that the L-band T_B H was affected by the snow properties of the top centimeters of the snowpack, in spite of the large penetration depth (hundreds of meters). Both the surface snow density and the thickness of the superficial layer were relevant, due to coherent interference effects.

Keywords: SMOS, Cryosphere, Microwave, Snow Emission Modeling.
Received 17 October 2016; Revised 10 July 2017; Accepted 30 July 2017; Online on doi.org/10.1016/j.rse.2017.07.035

1. Introduction

The physical properties of the surface are essential variables for understanding the surface energy and mass budgets of the Antarctic ice sheet and, in turn, for predicting climate change and the contribution of the ice sheet to a rise in the sea level. Several glaciological and meteorological properties are relevant, such as grain size, wetness, density, and roughness of snow, near surface air temperature, surface wind, and precipitations.

Because of the remoteness and the harsh conditions, satellite remote sensing is the sole means for acquiring long time-series of observations over the entire continent. In particular, microwave radiometers have been used in a wide range of applications to estimate snow properties and changes over the ice sheet, such as snow temperature (Surdyk, 2002; Schneider & Steig, 2002; Winebrenner et al., 2004), surface melting (Torinesi et al., 2003; Liu et al., 2006; Picard et al., 2007; Tedesco & Monaghan, 2009), mean annual snow accumulation (Zwally, 1977; Vaughan et al., 1999; Arthern et al., 2006), snow grain size (Brucker et al., 2010; Picard et al., 2012), surface and depth hoar detection (Hall et al., 1986; Shuman & Alley, 1993; Champollion et al., 2013) and roughness characteristics (Long & Drinkwater, 2000).

With penetration depths ranging from a few centimeters at 150 GHz to a few hundred meters at 1 GHz (Surdyk, 2002; Macelloni et al., 2016), the potential for probing both the surface and the internal structure at different levels in the ice sheet is important. During the past decade, the launching of various low-frequency radiometers operating at L-band (1.4 GHz) has opened up a new era. The European Space Agency (ESA)'s Soil Moisture and Ocean Salinity (SMOS) in 2009 (Kerr et al., 2010) was followed by the National Aeronautical and Space Agency (NASA)'s Aquarius in 2011 (Le Vine et al., 2010), which ceased operations in June 2015. NASA's Soil Moisture Active Passive (SMAP) was launched in 2015 (Entekhabi et al., 2010, 2014), and its radiometer has provided images since April 2015 (e.g. Chan et al., 2016; Roy et al., 2016). These missions were primarily dedicated to soil moisture and ocean salinity, but can however provide very interesting information on the ice sheet. Indeed, the penetration depth in dry snow and ice at L-band is estimated to be several hundred or thousand meters: that is, one order of magnitude greater than at 6 GHz, which is the next available frequency available from satellite observations (Surdyk, 2002; Tan et al., 2015; Macelloni et al., 2016).

Due to this penetration depth and to the unique characteristics of stability and homogeneity inside ice sheet, the Antarctic Plateau is a particularly suitable target for the calibration and validation of passive microwave satellites (Floury et al., 2002; Drinkwater et al., 2004; Macelloni et al., 2006). There is no doubt that the ice inside the ice sheet evolves only at century-time scales, and can be considered stable throughout the duration of a satellite mission (Macelloni et al., 2016). Closer to the surface, the penetration of the temperature wave is also very shallow compared to the penetration depth (Surdyk, 2002), with the result that the microwave

*Corresponding author
Email address: m.leduc@ifac.cnr.it (M. Leduc-Leballeur)

energy emitted by the snow and ice is only slightly modulated by seasonal and even inter-annual temperature variations (Macelloni et al., 2012; Leduc-Leballeur et al., 2015). In addition, because of the low accumulation rate (typically < 20 cm; Arthern et al., 2006), the low temperature and the dry snow (melting never occurs), the evolution in snow properties is much slower there than in any other region on earth. Lastly, some areas such as the domes and ridges feature low winds, meaning that snow redistribution processes are relatively limited and that the snowpack is relatively homogeneous (Van den Broeke & Van Lipzig, 2003; Libois et al., 2014; Picard et al., 2014).

The French-Italian Concordia station located at Dome C (75.06°S, 123.21°E) offers exceptional opportunities for monitoring snow and ice: numerous in situ atmospheric and snow measurements have in fact been obtained there over the past decade (e.g. Genthon et al., 2010; Lanconelli et al., 2011; Groot Zwaaftink et al., 2013; Libois et al., 2015; Picard et al., 2016). Moreover, specific campaigns dedicated to calibration at L-band have been conducted in order to collect snow properties at various depths (Leduc-Leballeur et al., 2015) and to measure L-band brightness temperature (T_B) using ground-based or airborne radiometers (Macelloni et al., 2013; Skou et al., 2015).

At Dome C, L-band T_B temporal variability is generally low (standard deviation: < 2 K), showing a variability at horizontal (H) polarization higher than at the vertical (V) one (Macelloni et al., 2013; Brucker et al., 2014b). The T_B H temporal variations observed by a ground-based L-band radiometer (DOMEX experiments) have shown a correlation with strong wind events (defined as periods when wind speed exceeds 7 m s^{-1} for several hours; Macelloni et al. (2013)). Aquarius T_B H analysis has also highlighted a correlation with the presence of hoar on the surface (Brucker et al., 2014b), something that had already been observed as affecting the higher frequencies (e.g. at Ka- and Ku-band in Shuman & Alley (1993) and Champollion et al. (2013)).

These features are usually explained by the transmission effect on the surface. Indeed, the microwave emission of the snowpack is attenuated at the snow-air interface (i.e. the surface)that is driven by the transmission coefficient (or, equivalently, by the reflection coefficient), which depends on the incidence angle. At V polarization, when the incidence angle is close to the Brewster's angle (i.e. about 55° for the ice sheet at L-band), the transmission coefficient is close to 1 and the surface characteristics have little influence on the T_B. In contrast, the H polarization coefficient is greatly influenced by the refractive index – which is mainly controlled by the snow density near the surface (in the microwave range and for dry snow) and, to some degree, by the surface roughness.

The objective of this study is to investigate the L-band T_B H temporal variation at Dome C by focusing on the 2014-2015 austral summer, during which a noticeable variation occurred compared to the 2010-2016 SMOS time-series. The effect of changes in snow surface properties during this period has been quantified by using a snow-emission model driven by time-series of in situ measurements. Here as follows, Section 2 introduces the SMOS observations, the atmospheric and snow measurements, and the snow-emission model. Section 3 describes the 2014-2015 austral summer in detail. Section 4 presents the modeling results. Lastly, the discussion and the conclusion are presented in Sections 5 and 6.

2. Data sets and Emission Model

The study is based on L-band T_B time-series measured by both the SMOS satellite and a ground-based radiometer (Section 2.1 and 2.2). To analyze the T_B variations, various data sets of snow and atmospheric properties have been used (Section 2.3). In particular, various in situ measurements are available via the French and Italian field teams (supported by the French Polar Institute (IPEV) and the National Antarctic Research Program (PNRA)), as well as via the American automatic weather station (AWS) at Dome C. These snow-property measurements were used as inputs for a snow-emission model (Section 2.4).

2.1. SMOS observations

The development of the SMOS mission was led by ESA in collaboration with the Centre National d'Etudes Spatiales (CNES) in France and the Centro para el Desarrollo Tecnologico Industrial (CDTI) in Spain. The SMOS satellite carries on board an L-band Microwave Imaging Radiometer with Aperture Synthesis (MIRAS) that operates at 1.4 GHz (21 cm) and has an average ground resolution of 43 km (McMullan et al., 2008). The radiometer provides a multi-angular fully polarized T_B (Kerr et al., 2010).

The SMOS Level 3 product contains multi-angular T_B at top of the atmosphere within the antenna polarization reference frame (Kerr et al., 2013; Al Bitar et al., 2017). The product is georeferenced on the Equal-Area Scalable Earth version 2.0 grid (EASE–Grid2; Brodzik et al. (2012)), and has an oversampled resolution of about 628 km^2. Grid points are distorted in the polar regions (around 100 x 6 km x km in meridian and zonal directions respectively). The product comprises daily-averaged and incident angle-averaged T_B with angle bins every 5° from 0° up to 65°. T_B V and T_B H at the grid point (75°08.4'S, 123°19.8'E) nearest to Dome C were extracted from January 2010 to June 2016. During the commissioning phase (January - May 2010), data were missing due to the specific mode of the instrument (calibration sequences, dual polarizations mode), which led to greater uncertainty for that particular period (Mecklenburg et al., 2012). The RE04 reprocessed version distributed by CATDS (Centre Aval de Traitement des Données SMOS; http://www.catds.fr/) was used.

The SMOS Level 3 product provides pixel radiometric accuracy estimated from the propagation of Level 1 associated radiometric accuracies (Al Bitar et al., 2017). At Dome C, the radiometric accuracy is 3.9 K on average, but depends on the incidence angle (Table 1). The present study focuses on incidence angles between 32.5° and 57.5° in order to benefit from an accuracy of less than 4 K. Incidence angles above 60° were not used due to their large ellipsoidal footprints (Kerr et al., 2012).

2.2. DOMEX ground radiometer

Since 2004, a ground-based RADOMEX L-band radiometer (1.413 GHz) has operated at Dome C during three successive campaigns entitled DOMEX-1, 2 and 3 (Macelloni et al., 2006, 2013). Their main objective was to evaluate the temporal stability of the SMOS for calibration purposes. These experiments were led by IFAC-CNR (Italy) in cooperation with the Italian space agency (PNRA) and ESA.

DOMEX-1 measurements were acquired over about 20 days, while both the DOMEX-2 and DOMEX-3 experiments lasted for 1.5 years and 3 years, respectively. For these latter experiments, measurements were acquired in general at a fixed incidence angle of 42°, which is the nominal observation angle for

Table 1: SMOS L3 Pixel Radiometric Accuracies (K) at Dome C from January 2010 to June 2016.

Incidence Angle (°)	2.5	7.5	12.5	17.5	22.5	27.5	32.5	37.5	42.5	47.5	52.5	57.5
T_B V Accuracy (K)	5.25	5.20	4.54	4.18	4.17	4.08	3.81	3.53	3.41	3.38	3.38	3.52
T_B H Accuracy (K)	5.24	5.14	4.49	4.20	4.20	4.05	3.77	3.47	3.35	3.31	3.29	3.40

the "browse product" of SMOS (Kerr et al., 2010). At this incidence angle, the footprint was 10 x 17 m^2. During the summer campaigns (i.e. from November to January), T_B was occasionally measured at different incident angles from 20° to 90°, every 10°, and periodic cold-sky observations were carried out. The radiometer accuracy was around 0.5 K. Data sets are available from https://earth.esa.int/web/guest/campaigns.

2.3. Snow and atmosphere properties

Surface snow density was measured at Dome C from October 2014 to May 2015. During the summer campaign, measurements were collected every day from 15 December 2014 to 15 January 2015. The frequency was reduced to every 2 to 7 days during the winter season. For every measurement session, five samples were taken in different locations chosen randomly within tens of meters in the "clean area",which is located about 500 m from the DOMEX radiometer. Only the averages of these 5 measurements are considered here. Density was measured with a 3 cm-thick cutter at two levels (0-3 cm and 3-6 cm) during the summer, but only at the 0-3 cm level during the winter (Libois et al., 2014).

Complementary measurements were collected deeper in the snow using a cylinder cutter that is 0.25 m high and has a diameter of 0.045 m. The measurements were performed at a depth of 0.1 m every 15 days in a stake farm composed of 8 stakes placed about 10 m from one another. The value used in this article is the mean of the 8 locations. The standard deviation ranged from 10 to 70 kg m^{-3}, exhibiting a typical value of around 40 kg m^{-3}. Lastly, density profiles were measured once a month in 1 m-deep snow pits every 10 cm.

Snow surface elevation was estimated by averaging measurements acquired by the Rugged Laser Scan installed at Dome C (Picard et al., 2016). This instrument provided daily maps of surface elevation over an area of 100 m^2 with a precision of about 1 cm and a horizontal resolution of 5 cm. It operated from January 2015 to January 2016. However, only data from February 2015 on are used here, because the stability of the platform was not satisfactory during the first month after its installation (Picard et al., 2016).

Snowfall was measured at Dome C from October 2014 to May 2015, with an interruption from 14 November 2014 to 14 December 2014. The measuring method is based on the daily measurement of the depth and the density of solid deposits on wooden tables 1 m above the surface (details in Groot Zwaaftink et al. (2013)). Edges 5 cm in height on 3 sides of the tables helped protect the deposits from being blown away by the wind. The density was measured by means of weighing. When the deposit of snow was too small for a reliable weight measurement, the density was estimated from the snow crystal forms. To this end, typical densities were inferred from the set of measurements: from 44 kg m^{-3} for needles (PPnd) up to 107 kg m^{-3} for small rounded particles (RGsr; for the abbreviations, see Fierz et al. (2009)).

Optical photographs provided pictures of the snow surface at Dome C every hour from October 2014 to May 2015. Photographs were taken with a heated webcam that had a 3-million-pixel resolution.

Wind speed in situ measurements at Dome C were provided by the automatic weather station (AWS) program of the Antarctic Meteorological Research Center (AMRC) at Dome C, a few kilometers from the snow density measurements. For this study, 3-hourly data were used to compute daily averages from 1996 to 2015 (available ftp://amrc.ssec.wisc.edu/pub/aws/antrdr/). Wind speed measurements had a resolution of 0.25 m s^{-1} and an accuracy of 0.5 m s^{-1} (Lazzara et al., 2012). Note that, due to the snow accumulation, the above-surface height of the sensors gradually decreased. Thus, the wind sensor height was 3 m in December 1995 and 1.45 m at the beginning of 2015. On 2 January 2015, a maintenance operation repositioned the wind sensor at 2.5 m above the surface (cf. the field report AMRC, 2015). Linear regression, which was performed from 1996 to December 2014, gave -7 10^{-5} m s^{-1} $\pm$ 1 10^{-5} m s^{-1}, thus suggesting the effect of height variation could be disregarded in this study.

ERA-Interim reanalysis produced by the European Centre for Medium-Range Weather Forecasts (ECMWF; Dee et al. (2011)) was also used to map 10-m wind speed during the 2014-2015 austral summer.

2.4. Snow microwave emission model

Modeling L-band snow emission in Antarctica has been dealt with in several studies in which the specificity of the snow-wave interaction at a low frequency was highlighted (Brogioni et al., 2015; Jezek et al., 2015; Leduc-Leballeur et al., 2015; Tan et al., 2015). The simulations performed at Dome C showed that the snow density profile is the second most important driver of the T_B after snow/firn/ice temperature, whereas grain size is usually most relevant at higher frequencies (e.g. Brucker et al., 2010). In particular, the main cause of scattering in the medium is layering, i.e. the small variations in density that are observed between each successive layer. In fact, even if each single interface causes only a small reflection due to the weak contrast in the refractive index, the number of layers crossed by the waves is very high because the penetration depth is a few hundred meters and the typical layer thickness is less than 8 cm (the annual accumulation amount). Therefore, particular attention is required in order to take into account the inter-layer variability of density (Leduc-Leballeur et al., 2015).

Moreover, since the thickness of the layers is of the order of the wavelength, interferences between the multiple waves resulting for the numerous reflections are significant. The electromagnetic wave-theory makes it possible to predict interferences, because it explicitly computes the phase of the electric field during the propagation within the medium (West et al., 1996; Tsang et al., 2000). For this reason, the WALOMIS (Wave Approach for LOw-frequency MIcrowave emission in Snow) multilayer emission model is used here (Leduc-Leballeur et al., 2015). This model describes the snow, firn and ice as a stack of plane-parallel layers characterized by their thickness, temperature, and density. Scattering by snow grains is disregarded, since the wavelength at L-band is several orders of magnitude larger than the grain size (Mätzler, 1987).

To correctly predict the interferences using a wave-theory model, it is important to represent the natural variability (randomness) on the footprint scale of the sensor (i.e. ∼43 km wide for SMOS). For this purpose, several runs were processed with slightly different stacks of layers and the results were then averaged. It is necessary that the set of stacks represent the said natural variability, but it is impossible to obtain it from direct measurements of the density profile. Instead, West et al. (1996) proposed a stochastic model designed and calibrated from the statistical properties of a few observed profiles. Similar approaches have been used in Brogioni et al. (2015) and Tan et al. (2015). The West et al. (1996) approach was applied at Dome C in Leduc-Leballeur et al. (2015) from ten cores measuring 11-80 m in length, which corresponded to the ice sheet part in which the density was the most variable. They extrapolated the measured profiles down to 3200 m depth to provide realistic snow characteristics all the way down to the bedrock, which were essential due to the large penetration depth at L-band. They generated 10 000 density profiles and used them to simulate successfully the T_B observed by SMOS at Dome C with WALOMIS. Here, the same 10 000 density profiles were used again, but with certain adaptations to account for surface variability.

The ice permittivity complex value is critical for simulations at L-band. The real part is fairly constant over the microwave range, and depends on snow density but not on temperature. Its value is considered to be known with sufficient accuracy. In contrast, the imaginary part is extremely uncertain, and has a stronger dependency on temperature. The imaginary part controls the absorption and, hence, the penetration depth. At Dome C, Leduc-Leballeur et al. (2015) and Macelloni et al. (2016) applied two formulations (Tiuri et al. (1984) and Mätzler (1987, 2006)), which differed by a factor 5 at 1.4 GHz. The results showed that the former formulation yielded results closer to the SMOS observations in terms of absolute T_B and polarization ratio. For the present study, simulations were performed using both formulations and the results confirmed a systematic bias of 3-6 K (depending on the incidence angle) with the Mäztler's formulation. However, the magnitude of the temporal variations was exactly the same with both formulations. This indicated that the results presented here as follow are independent of the permittivity choice. For the sake of simplicity and due to lesser bias with the Tiuri's formulation, only the results for this formulation are provided.

3. Description of the 2014-2015 austral summer

At Dome C during the period from June 2010 to June 2016, the mean SMOS T_B at 52.2° incidence angle was 217.3 K ± 0.7 K and 179.9 K ± 1.5 K at V and H polarization, respectively (Fig. 1). Thus, the L-band T_B has been relatively stable since 2010, as expected for the inner part of Antarctica (Macelloni et al., 2012; Brucker et al., 2014a). DOMEX T_B collected at 42° from 2010 to 2016 showed a similar stability of 0.42 K and 1.72 K at V and H polarizations, respectively. This also confirmed the higher variability at H polarization compared to the V polarization already observed in this area (e.g. Brucker et al., 2014b). The temporal trend at H polarization was 7 10^{-5} K ± 7 10^{-5}, which actually is not significantly different from zero (p=0.32).

During the 2014-2015 austral summer, an important change occurred in the Dome C area: T_B H increased to around 186 K, a result never reached during the 6-year period of available observations, and then sharply decreased within a few days. Another similar event occurred during the austral summer of 2010-2011,

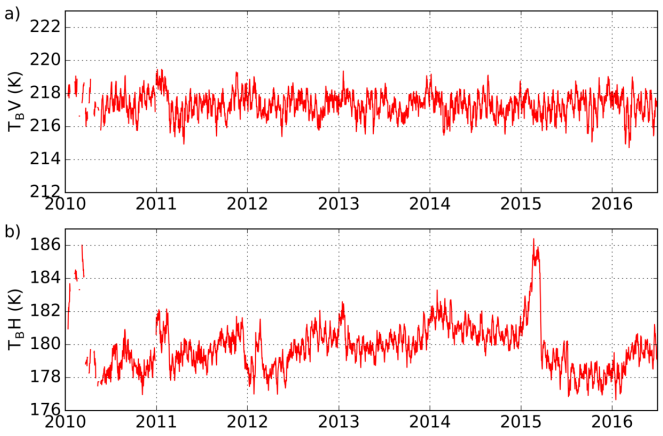

Figure 1: SMOS T_B (K) at Dome C, Antarctica from January 2010 to June 2016 for 52.5° incidence angle at (a) V and (b) H polarization.

one which coincided with the early stage of the SMOS mission. Despite the great uncertainties in the sensor's performances during this phase, the magnitude was significant and the event was confirmed by the DOMEX measurements. Here, only the 2015 event was investigated, because of the lack of available in situ measurements required to run the snow-emission model in 2010.

Fig. 2 shows the variations from October 2014 to May 2015. The T_B H observed by SMOS featured a progressive increase of about 3-5 K (depending on the incidence angle) from mid-December 2014 to March 2015, followed by a sharp decrease at the end of March 2015. This decrease was estimated to be 3.5 K, 4.0 K and 5.4 K at 32.5°, 42.5° and 52.5°, respectively, between 16 and 23 March 2015. With a smaller spatial resolution and a higher temporal resolution than the SMOS observations, the DOMEX observations recorded the beginning of the increase in T_B H from November on and a similar decrease of 5.4 K at 42° estimated over 2 days, starting from 20 March 2015.

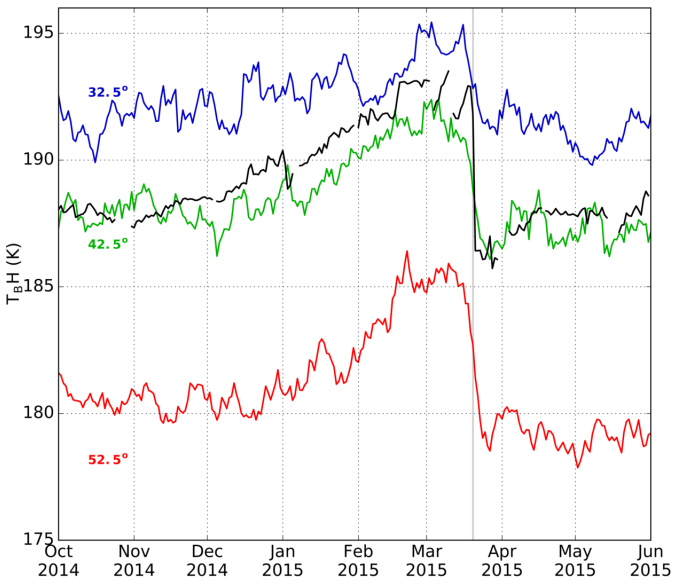

Figure 2: T_B H (K) at Dome C, Antarctica from October 2014 to May 2015 with SMOS at 32.5° (blue), 42.5° (green) and 52.5° (red) incidence angle, and with DOMEX at 42° (black).

Both SMOS and DOMEX observed simultaneous variations, ones that ruled out any particular defect in the sensors. In addition, the similar magnitude suggests that the event had a rel-

ative homogeneous effect ranging from the small scale – a few hundred meters around the DOMEX radiometer – to the SMOS pixel of 628 km^2. This could be further confirmed by the spatial analysis presented in Fig. 3. A rapid decrease greater than 2 K at 52.5° was recorded in 97 SMOS pixels in the Dome C vicinity, i.e. about 60 000 km^2. Over the same period, T_B V remained constant, which indicated that the changes affected only the surface.

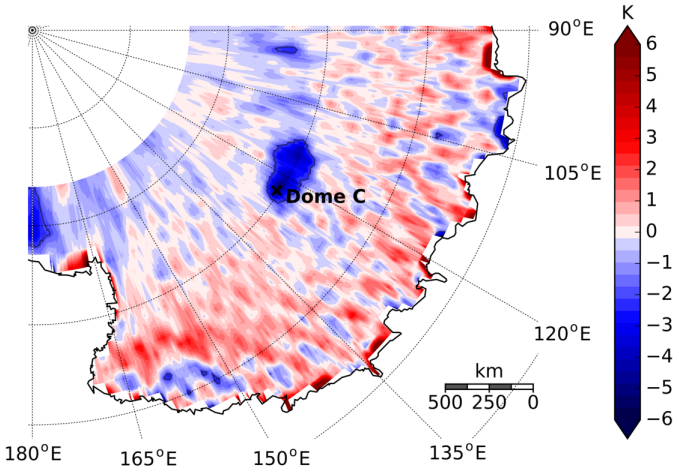

Figure 3: Difference between SMOS T_B H (K) averaged over ten days after and ten days before 20 March 2015. Grey line is the - 2 K contour.

Meteorological and glaciological in situ measurements were analyzed in order to depict the conditions during this event. In Fig. 4a, the snow density measured in the top 3 centimeters showed a continuous decrease from 300 kg m^{-3} in November 2014 down to 150 kg m^{-3} in March 2015, which is a very low snow density with respect to the usual surface snow density at Dome C of about 300 kg m^{-3}. Around 20 March 2015, the density rapidly increased up to 300 kg m^{-3}, which was similar to the measurements taken at the beginning of the summer. In contrast, the few measurements performed at a depth of between 3 and 10 cm did not capture any variation during that period: in fact, the density remained around 300 kg m^{-3} (Fig. 4a, grey points). This suggested that only the density in the uppermost 3 cm of the snowpack decreased during the 2014-2015 summer, and that therefore no sharp increase could be expected below this superficial layer.

This was indirectly confirmed by the snow surface elevation measured by the Rugged Laser Scan (Fig. 4b) and by the surface wind speed (Fig. 4c). The surface elevation increased progressively by 2.5 cm from February on and until 20 March 2015. This slow growth could due both to the development of hoar on the surface and to the accumulation of light snow, both favored by a low wind speed. Indeed, from November 2014 to February 2015, the wind speed was 2.4 m s^{-1} on average, which was 0.5 m s^{-1} lower than the climatology for those same months from 1996 to 2015. Moreover, Champollion et al. (2013) pointed out that weak wind conditions were favorable to the growth of hoar and that the removal of this fragile layer required a wind speed stronger than 4 m s^{-1}. Analysis of daily wind speed for the 1996-2015 period, showed that strong winds (stronger than 4 m s^{-1}) occurred 45% less than usual at this time, from December 2014 to February 2015. The presence of hoar was also clearly illustrated by the daily photographs of the surface at Dome C from the beginning of December (cf. Dome C time-lapse photographs).

Snowfalls are rare from January to mid-February 2015 (Fig. 4b). However, a particularly heavy snowfall took place on 18 February 2015, concomitant with the minimum of surface density. From 18

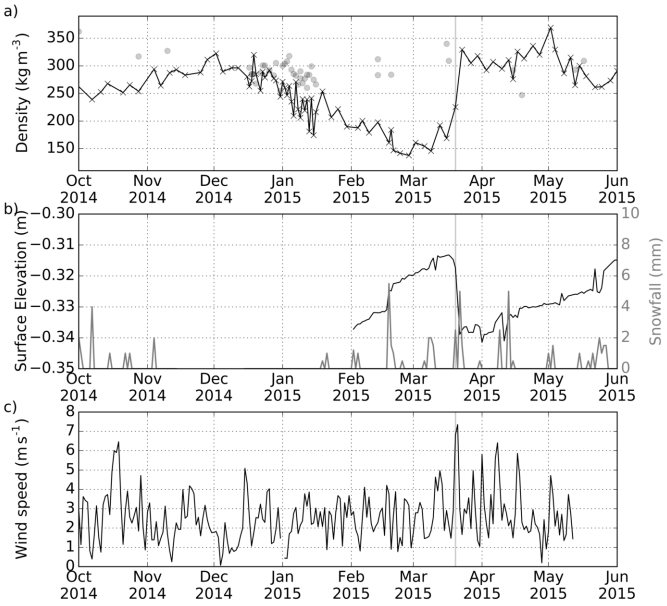

Figure 4: (a) Snow density (kg m^{-3}) measured on the surface (0–3 cm depth; line) and below (3–6 cm depth, grey points); (b) Surface elevation (m, black) estimated from Rugged Laser Scan and snowfall in situ measurements (mm, grey); (c) Surface wind speed (m s^{-1}), at Dome C, Antarctica.

February 2015 on, daily photographs also highlighted changes on the surface, which suggest a mixed layer made up of hoar and light snow, up until 20 March 2015.

On 20 March 2015, 2 cm of snow were suddenly removed over the space of one or two days (Fig. 4b). The daily photographs of Dome C from 18 to 23 March 2015 highlighted the changes in the surface and confirmed the lowering of the surface by a few cm (Fig.5). This decrease could be attributed to erosion of the superficial layer as a consequence of the strong wind event of that day (about 7 m s^{-1}, Fig. 4c).

Overall, the account depicted by the observations was qualitatively coherent, and highlighted the simultaneity of the snow properties and T_B H variations. The density increased due to the removal of a light layer accumulated or formed during the summer. The reflection coefficient at H polarization increased as a consequence of the change in the refractive index, which explains why only T_B H decreased. The following section will deal will this question from a quantitative point of view.

4. Effect of variations in surface snow properties

The WALOMIS snow-emission model was used to simulate L-band T_B H from the time-series of snow properties in the superficial layer.

4.1. Surface snow density

As a first step, only the variations in snow density were considered. The model was run with a 3-cm layer with time-varying properties on top of the snowpacks used in Leduc-Leballeur et al. (2015). The density of this superficial layer was obtained from the in situ measurements (Fig. 4a). Fig. 6a shows the simulations compared to the SMOS observations at 32.5°, 42.5° and 52.5° incidence angle. The root-mean-square error (RMSE) ranged from 1 K to 4.4 K, depending on the incidence angle (RMSE1 in Table 2). The weak increase in T_B H during the summer period was correctly predicted until February at all incidence angles. However, the simulated T_B H remained constant from February on, while

Figure 5: Dome C area photographs from 18 to 23 March 2015 between 10 h and 12 h, with a focus on the base of sensor at the bottom right. Red bands are spaced about 5 cm.

the SMOS observations continued to increase, leading to a difference of 5 K at 52.5° on 19 March 2015. Consequently, the model underestimated the magnitude of the increase. The decrease in T_B H around 20 March 2015 was well captured by the model. This was expected because the density of the superficial layer had nearly doubled. The difference between the simulations and the observations after this decrease became very small, i.e. similar to the summer period. At the end of the period, the T_B H was very close to what it had been at the beginning: i.e. the mean T_B H at 52.5° was 180.5 K and 177.8 K in November 2014 for SMOS and the model, and 179.3 K and 177.0 K, respectively, in April 2015.

The simulations were slightly biased during this period, particularly at large incidence angles. This condition had already been noted in the first application of WALOMIS at Dome C in Leduc-Leballeur et al. (2015). The bias estimated from this study reached as much as 5.2 K at 57.5° (Table 2). The RMSE computed from unbiased simulations ranged from 1 K to 1.7 K, a result that emphasized the agreement with the SMOS observations (RMSE1-ub in Table 2).

These results demonstrated the strong influence of the density of the first centimeters of snowpack on the L-band signal, although the wavelength was much larger than this superficial layer. The disagreement between the simulations and the observations in February and March 2015, when the surface snow density was

at its lowest (somewhat less than 200 kg m^{-3}), is surprising because, while the density continued to decrease in February (Fig. 4), the T_B H did not vary accordingly. This suggests that the influence of density on the T_B H saturated at low values and/or that another snow parameter was needed to explain the variations.

4.2. Thickness of the superficial layer

The changes in the surface elevation observed (Fig. 4b) clearly showed that the hypothesis of a superficial layer with a constant 3-cm thickness was unrealistic. In this section, the surface elevation changes were taken into account in the simulations, together with the density variations, by assuming that only the thickness and the density of the superficial layer changed. The other properties in the top layer and all the properties of the layers below remained constant through the time-series. The thickness of the superficial layer was estimated using the Rugged Laser Scan measurements (Fig. 4), available from February to May 2015.

Since the Rugged Laser Scan measured elevation change, the initial thickness of this layer was unknown. Several tests were performed with a 3-, 4- and 5-cm initial thickness. They showed a low impact on the simulations (the overall RMSE between simulations and observations were, respectively, 1.5 K, 1.4 K, 1.3 K across all the incidences angles). On the contrary, using 1 or 2 cm strongly reduced the magnitude of the temporal variations, and the simulations agreed less with the observations (the RMSE were 1.9 K and 2.6 K, respectively). Here as follows, an initial thickness of 3 cm is considered, so as to be consistent with the previous section. The choice was also supported by the fact that the density under this depth did not change during the entire period, as indicated by the in situ measurements (Fig. 4a).

The WALOMIS simulations, including the thickness variations, are in better agreement with the observations (Fig. 6b), compared to the simulations with a constant thickness performed in the previous section (Fig. 6a). The increase in T_B H between February and March 2015 is well represented, as well as the decrease of 20 March 2015. The overall RMSE between observations and simulations improved at all angles, except at 32.5°, where it slightly increased (RMSE2 in Table 2). RMSE were also estimated from unbiased simulations (RMSE2-ub in Table 2). However, note that RMSE2 and RMSE2-ub were computed with 35 points for each incidence angle, which was not enough to be absolutely reliable.

Table 2: T_B H RMSE (K) at Dome C estimated from SMOS and various WALOMIS simulations as described in Section 4. Bias (K) estimated from Leduc-Leballeur et al. (2015).

Incidence Angle (°)	32.5	37.5	42.5	47.5	52.5	57.5
RMSE1 (K)	1.2	1.0	1.3	1.7	2.7	4.4
RMSE2 (K)	1.7	1.0	1.2	1.5	2.1	3.3
Bias (K)	-0.7	0.0	1.6	1.8	2.1	5.2
RMSE1-ub (K)	1.0	1.0	1.4	1.5	1.4	1.7
RMSE2-ub (K)	1.2	1.0	1.8	2.0	1.5	2.8

5. Discussion

The WALOMIS snow-emission model required three parameters to describe each layer of the snowpacks: temperature, density and thickness. Leduc-Leballeur et al. (2015) suggested that the seasonal temperature variations in the first ten meters of snowpack would not affect the L-band T_B at Dome C. Indeed, their simulations, which were performed with summer and winter temperature profiles, showed a mean difference of only 0.21 K at V polarization and 0.33 K at H polarization, although the temperature varied by about 35°C on the surface and less than 10°C at 2 m depth between the two seasons. Thus, only density and thickness could explain the significant variation observed in the L-band T_B H. Fig. 7 shows the theoretical sensitivity of the WALOMIS simulations to these two parameters at H polarization. In the 100-300 kg m^{-3} surface density range, the T_B H increased along with the thickness. The increase was more pronounced for surface densities of around 150-200 kg m^{-3}, and tended to disappear for surface densities of close to 340 kg m^{-3}. For a 1-2 cm layer thickness, T_B H varied little with the changes in the surface density. For a greater layer thickness, an increase in T_B H was observed followed by a decrease when the surface density increased. This was due to a coherent effect that generated a resonance in the emission, which depended on both the layer thickness and the wavelength on the media. The latter depended on the permittivity, which in turn depended on density. In brief, this sensitivity test confirmed that, in this density range, a combination of decreasing density and increasing thickness led to an increase in the T_B H.

The low wind-speed conditions recorded by the in situ measurements between November 2014 and March 2015 facilitated the presence of low-density snow, and so favored the growth of the superficial layer. A storm that occurred on 20 March 2015 removed (or compacted) this recent layer, and enabled a dense snow layer emerge on the surface. This scenario was confirmed by density and surface elevation measurements, as well as by photographs of the snow surface taken at the site (Fig. 5). Simulations with the snow-emission model showed that the change in density explains part of the T_B H variations during this period. However, only the thickness and the density variations together can fully explain the observations. This result is remarkable in that it is specific to the low frequency. Indeed, the sensitivity to the thickness arose because the layer thickness was minor as compared to the wavelength (about 3-5 cm versus 21 cm). In this case, the effective reflectivity of the snowpack was not only controlled by the Fresnel coefficients, but also by the thickness of the layer relative to the wavelength (Wiesmann & Mätzler, 1999; Mätzler, 1987; Tsang et al., 2000). Only the wave theory was able to predict this behavior. The radiative theory was not able to do so, except when an ad hoc treatment of the reflection coefficient was specifically applied (Wiesmann & Mätzler, 1999). The simulations performed with the DMRT-ML radiative transfer model (Picard et al., 2013) – which does not include this treatment – confirmed the insensitivity to the layer thickness (not shown here). Because of this inter-dependency between density and thickness, the retrieval of surface information from L-band T_B observations was more rigorously under-constrained than if only density variations had contributed to the T_B variations. For instance, it seems complex to retrieve the snow surface density and the snow accumulation using L-band observations alone when such small layers may be present (Lemmetyinen et al., 2016).

Understanding the link between snow properties and T_B was the main achievement obtained from the results presented, but additional investigations will be needed to fully understand the 2014-2015 austral summer events from the point of view of both snow and meteorology. The first point is the rarity of the event. At high microwave frequencies, rapid changes in T_B H are frequent and have been partially explained by the cycles of slow formation / rapid disappearance of hoar on the surface (Shuman & Alley, 1993; Champollion et al., 2013). Thus, 19 GHz and 37 GHz polarization ratios usually show an increase every summer at Dome C. Although the hoar layer can be as much as 2 cm in thickness and

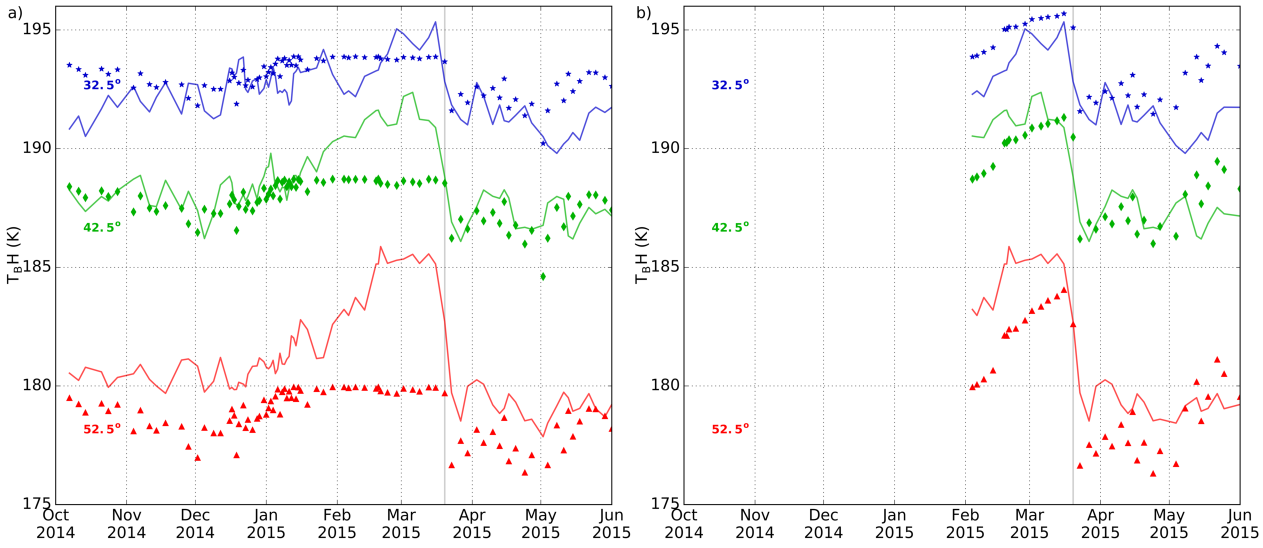

Figure 6: T_B H (K) at Dome C, Antarctica from October 2014 to May 2015 at 32.5° (blue), 42.5° (green) and 52.5° (red) incidence angle with SMOS (lines) and WALOMIS simulations (symbols) (a) taking into account the surface snow density variations and (b) taking into account both the variations of surface snow density and surface elevation.

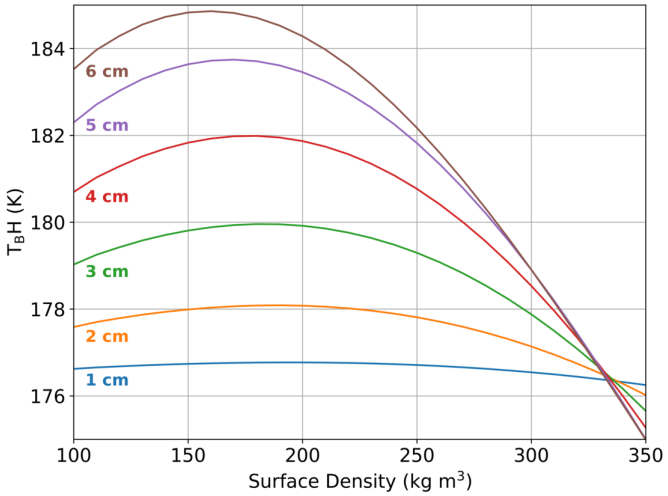

Figure 7: T_B H (K) WALOMIS simulations as a function of density in the top layer of the snowpack for layer thickness from 1 to 6 cm.

generally has a low density, one that is similar to the properties of the superficial layer measured in February, these events are detectable but weak at L-band (Brucker et al., 2014b). The said weakness may be explained by the diminutive thickness of the layer compared to the wavelength at L-band versus high frequencies. In contrast, the variations in T_B during the 2014-2015 austral summer were extensive at L-band, an occurrence that is very rare and indicates that particular conditions occurred during that period. In this regard, the lower than normal daily wind speed observed over five months could be favorable both to the snow accumulation and to a particularly long period of hoar development. The hoar gradually thickened up to become detectable at L-band. According to the time-series of photographs and to scientists in the field, exceptional hoar development was observed during the 2009-2010 and 2014-2015 summers at Dome C, observations that were consistent with the two maxima of T_B H observed (Fig. 1). This suggested that the presence of hoar was a key element in this event. Lastly, when the strong wind event occurred, a low-density layer was removed and significant changes in the surface occurred with the formation of sastrugi and the deposit of fresh snow (Fig. 5).

Another point to be investigated concerns the spatial extent of the change. Fig. 3 shows that the extent was very well delineated and relatively small compared to the Antarctica size. The wind maps from the ERA Interim reanalysis during the period revealed the presence of a storm in the vicinity of Dome C (e.g. Fig. 8), which probably permitted the T_B H change. However, although similar and higher wind speeds were found in other places that very same day, no particular change in the SMOS signal was observed. Moreover, the wind pattern around Dome C was clearly different from that of the T_B H decrease pattern. This suggests that the strong wind event was not the only factor triggering the T_B H change and that the meteorological conditions over the previous months also played a key role.

Both points highlight the particular and complex conditions that made the L-band change possible on 20 March 2015, and explain the rarity of such an event. A combination of several factors is probably involved, as well as a specific sequence of changes that began during the 2014-2015 austral summer when the T_B H started to increase outside of its normal range. The storm was only the trigger for a return to normal conditions.

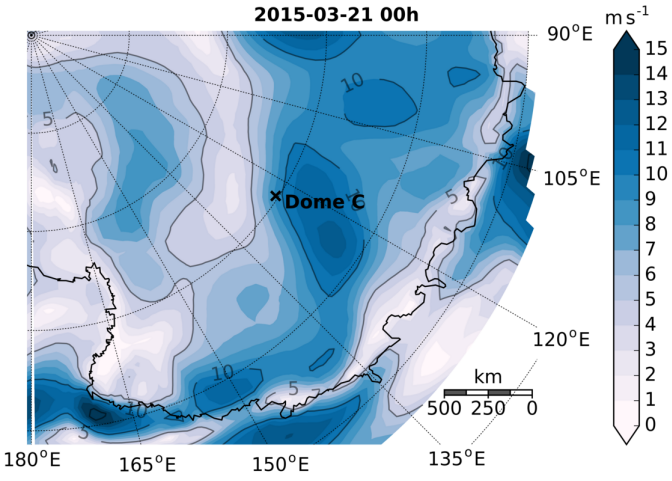

Figure 8: 10-m wind speed (m s^{-1}) on 21 March 2015 at 0 h from ERA-Interim reanalysis.

6. Conclusion

The six years of Earth monitoring from the SMOS satellite showed the stability of L-band T_B at Dome C in Antarctica. However, unexpected variations were observed twice at H polarization during this period. In situ snow properties and weather measurements at Dome C simultaneously showed significant variations.

From November 2014 to March 2015, the slow increase in T_B H occurred concomitantly with a decrease in surface snow density. During this period, low wind speed made the presence of hoar and the accumulation of light snow possible. Around 20 March 2015, an abrupt decrease in T_B H was observed (higher than 5 K at 52.5° incidence angle) and corresponded with a clear increase in surface snow density. Strong wind was also observed, a fact which could have compacted or removed the light snow presents on the surface.

The WALOMIS snow-emission model, which is based on the wave-theory, was used to investigate the change in snow properties that could explain these exceptional variations. As a first step, the simulations only considered the variations in surface snow density measured at Dome C. A good agreement was obtained between the simulations and the SMOS observations for part of the period, which suggests that T_B H was affected by a change in surface density. However, to completely reproduce T_B H variations, it was necessary to account for the variations in the surface layer thickness. Daily measurements of the surface elevation were used to estimate the variation in the layer thickness. The simulations, which took into account snow density and surface layer thickness variations together, showed very satisfying agreement with the observations.

These results confirmed that T_B H was influenced by the snow properties of the first centimeters in spite of the large penetration depth at L-band (several hundreds of meters (Macelloni et al., 2016)). More importantly, this showed that the thickness of the superficial layer is an important factor, which is a specific feature of the low frequency that results from interference phenomena. Radiative transfer theory does not predict such a dependence on the thickness, and is in principle inadequate for describing layers smaller than the wavelength. We therefore recommend using the wave theory approach in the lower part of the microwave domain.

The causes of the changes on the snow surface that resulted in the exceptional T_B H changes are complex and are only partially elucidated here. They are linked to an exceptional hoar formation during the summer, as well as to snow accumulation. Both were made possible by weaker than normal wind, which prevailed for long periods before 20 March 2015. A layer of light snow very probably grew until its thickness became sufficient to be detected at L-band. The extension of this study to the whole continent is an interesting perspective, but could be challenging because of the limited in situ measurements available at the scale of Antarctica.

Acknowledgments

This study benefited from financial support from ESA through CryoSMOS project and from the French space agency (CNES) through the SMOS TOSCA project. The authors acknowledge the French Polar Institute (IPEV) and the National Antarctic Research Program (PNRA) for financial and logistical support at Concordia station in Antarctica through the NIVO, MAISARS and MAPME programs, as well as H. Fréville for the intensive measurements period at Dome C. The SMOS product was obtained from CATDS, operated for the CNES by IFREMER (Brest, France). The UW-Madison AWS Program provided in situ measurements data set.

References

Al Bitar, A., Mialon, A., Kerr, Y., Cabot, F., Richaume, P., Jacquette, E., Quesney, A., Mahmoodi, A., Tarot, S., Parrens, M., Al-yaari, A., Pellarin, T., Rodriguez-Fernandez, N., & Wigneron, J.-P. (2017). The Global SMOS Level 3 daily soil moisture and brightness temperature maps. *Earth System Science Data Discussions*, . doi:10.5194/essd-2017-1.

AMRC (2015). *Wisconsin Team AWS Field Season 2014-15 Notes*. Technical Report. URL: http://amrc.ssec.wisc.edu/aws/documents/fieldreports/aws_fldrpt1415.pdf.

Arthern, R. J., Winebrenner, D. P., & Vaughan, D. G. (2006). Antarctic snow accumulation mapped using polarization of 4.3-cm wavelength microwave emission. *J. Geophys. Res.*, *111*. doi:10.1029/2004JD005667.

Brodzik, M. J., Billingsley, B., Haran, T., Raup, B., & Savoie, M. H. (2012). EASE-grid 2.0: Incremental but Significant Improvements for Earth-Gridded Data Sets. *ISPRS International Journal of Geo-Information*, *1*, 32–45. doi:10.3390/ijgi1010032.

Van den Broeke, M. R., & Van Lipzig, N. P. M. (2003). Factors Controlling the Near-Surface Wind Field in Antarctica. *Monthly Weather Review*, *131*, 733–743.

Brogioni, M., Macelloni, G., Montomoli, F., & Jezek, K. C. (2015). Simulating Multifrequency Ground-Based Radiometric Measurements at Dome C — Antarctica. *IEEE Journal of Selected Topics in Applied Earth Observations and Remote Sensing*, *8*, 4405–4417. doi:10.1109/JSTARS.2015.2427512.

Brucker, L., Dinnat, E. P., & Koenig, L. S. (2014a). Weekly gridded Aquarius L-band radiometer/scatterometer observations and salinity retrievals over the polar regions — Part 2: Initial product analysis. *The Cryosphere*, *8*, 915–930. doi:10.5194/tc-8-915-2014.

Brucker, L., Dinnat, E. P., Picard, G., & Champollion, N. (2014b). Effect of snow surface metamorphism on Aquarius L-band radiometer observations at Dome C, Antarctica. *IEEE Trans. Geosci. Remote Sens.*, *52*, 7408–7417. doi:10.1109/TGRS.2014.2312102.

Brucker, L., Picard, G., & Fily, M. (2010). Snow grain-size profiles deduced from microwave snow emissivities in Antarctica. *J. Glaciol.*, *56*, 514–526. doi:10.3189/002214310792447806.

Champollion, N., Picard, G., Arnaud, L., Lefebvre, E., & Fily, M. (2013). Hoar crystal development and disappearance at Dome C, Antarctica: observation by near-infrared photography and passive microwave satellite. *The Cryosphere*, *7*, 1247–1262. doi:10.5194/tc-7-1247-2013.

Chan, S. K., Bindlish, R., O'Neill, P. E., Njoku, E., Jackson, T., Colliander, A., Chen, F., Burgin, M., Dunbar, S., Piepmeier, J., Yueh, S., Entekhabi, D., Cosh, M. H., Caldwell, T., Walker, J., Wu, X., Berg, A., Rowlandson, T., Pacheco, A., McNairn, H., Thibeault, M., Martínez-Fernández, J., González-Zamora, A., Seyfried, M., Bosch, D., Starks, P., Goodrich, D., Prueger, J., Palecki, M., Small, E. E., Zreda, M., Calvet, J. C., Crow, W. T., & Kerr, Y. (2016). Assessment of the SMAP Passive Soil Moisture Product. *IEEE Trans. Geosci. Remote Sens.*, *54*, 4994–5007. doi:10.1109/TGRS.2016.2561938.

Dee, D. P., Uppala, S. M., Simmons, A. J., Berrisford, P., Poli, P., Kobayashi, S., Andrae, U., Balmaseda, M. A., Balsamo, G., Bauer, P., Bechtold, P., Beljaars, A. C. M., van de Berg, L., Bidlot, J., Bormann, N., Delsol, C., Dragani, R., Fuentes, M., Geer, A. J., Haimberger, L., Healy, S. B., Hersbach, H., Hólm, E. V., Isaksen, L., Kållberg, P., Köhler, M., Matricardi, M., McNally, A. P., Monge-Sanz, B. M., Morcrette, J.-J., Park, B.-K., Peubey, C., de Rosnay, P., Tavolato, C., Thépaut, J.-N., & Vitart, F. (2011). The ERA-Interim reanalysis: Configuration and performance of the data assimilation system. *Quart. J. Roy. Meteor. Soc.*, *137*, 553–597. doi:10.1002/qj.828.

Drinkwater, M. R., Floury, N., & Tedesco, M. (2004). L-band ice-sheet brightness temperatures at Dome C, Antarctica: spectral emission modelling, temporal stability and impact of the ionosphere. *Ann. Glaciol.*, *39*, 391–396. doi:10.3189/172756404781814014.

Entekhabi, D., Njoku, E. G., O'Neill, P. E., Kellogg, K. H., Crow, W. T., Edelstein, W. N., Entin, J. K., Goodman, S. D., Jackson, T. J., Johnson, J., Kimball, J., Piepmeier, J. R., Koster, R. D., Martin, N., McDonald, K. C., Moghaddam, M., Moran, S., Reichle, R., Shi, J. C., Spencer, M. W., Thurman, S. W., Tsang, L., & Van Zyl, J. (2010). The soil moisture active passive (SMAP) mission. *Proc. IEEE*, *98*, 704–716. doi:10.1109/JPROC.2010.2043918.

Entekhabi, D., Yueh, S., O'Neill, P., & Kellogg, K. (2014). SMAP handbook. *JPL Publication JPL*, (pp. 400–1567).

Fierz, C., Armstrong, R., Durand, Y., Etchevers, P., Greene, E., McClung, D., Nishimura, K., Satyawali, P., Sokratov, S., & der Künste ZHdK, Z. (2009). IACS international classification for seasonal snow on the ground. *International Association of Cryospheric Sciences, UNESCO, Paris*, .

Floury, N., Drinkwater, M., & Witasse, O. (2002). L-band brightness temperature of ice sheets in Antarctica: Emission modelling, ionospheric contribution and temporal stability. *Geoscience and Remote Sensing Symposium, 2002.*

IGARSS'02. 2002 IEEE International, *4*, 2103–2105. doi:10.1109/IGARSS.2002.1026458.

Genthon, C., Town, M. S., Six, D., Favier, V., Argentini, S., & Pellegrini, A. (2010). Meteorological atmospheric boundary layer measurements and ECMWF analyses during summer at Dome C, Antarctica. *Journal of Geophysical Research: Atmospheres*, *115*. doi:10.1029/2009JD012741.

Groot Zwaaftink, C., Cagnati, A., Crepaz, A., Fierz, C., Macelloni, G., Valt, M., & Lehning, M. (2013). Event-driven deposition of snow on the Antarctic Plateau: analyzing field measurements with SNOWPACK. *The Cryosphere*, *7*, 333–347. doi:10.5194/tc-7-333-2013.

Hall, D., Chang, A., & Foster, J. (1986). Detection of the depth-hoar layer in the snow-pack of the Arctic coastal plain of Alaska, USA, using satellite data. *Journal of Glaciology*, *32*, 87–94. doi:10.3198/1986JoG32-110-87-94.

Jezek, K. C., Johnson, J. T., Drinkwater, M. R., Macelloni, G., Tsang, L., Aksoy, M., & Durand, M. (2015). Radiometric approach for estimating relative changes in intraglacier average temperature. *IEEE Trans. Geosci. Remote Sens.*, *53*, 134–143. doi:10.1109/TGRS.2014.2319265.

Kerr, Y. H., Jacquette, E., Al Bitar, A., Cabot, F., Mialon, A., Richaume, P., Quesney, A., & Berthon, L. (2013). *CATDS SMOS L3 soil moisture retrieval processor – Algorithm Theoretical Baseline Document (ATBD)*. Technical Report SO-TN-CBSA-GS-0029, Issue 2.e. URL: http://www.cesbio.ups-tlse.fr/SMOS_blog/wp-content/uploads/2013/08/ATBD_L3_rev2_draft.pdf.

Kerr, Y. H., Waldteufel, P., Richaume, P., Wigneron, J. P., Ferrazzoli, P., Mahmoodi, A., Al Bitar, A., Cabot, F., Gruhier, C., Juglea, S. E., Leroux, D., Mialon, A., & Delwart, S. (2012). The SMOS Soil Moisture Retrieval Algorithm. *IEEE Trans. Geosci. Remote Sens.*, *50*, 1384–1403. doi:10.1109/TGRS.2012.2184548.

Kerr, Y. H., Waldteufel, P., Wigneron, J.-P., Delwart, S., Cabot, F., Boutin, J., Escorihuela, M.-J., Font, J., Reul, N., Gruhier, C., Juglea, S. E., Drinkwater, M. R., Hahne, A., Martín-Neira, M., & Mecklenburg, S. (2010). The SMOS mission: New tool for monitoring key elements ofthe global water cycle. *Proc. IEEE*, *98*, 666–687. doi:10.1109/JPROC.2010.2043032.

Lanconelli, C., Busetto, M., Dutton, E., König-Langlo, G., Maturilli, M., Sieger, R., Vitale, V., & Yamanouchi, T. (2011). Polar baseline surface radiation measurements during the International Polar Year 2007–2009. *Earth System Science Data*, *3*, 1–8. doi:10.5194/essd-3-1-2011.

Lazzara, M. A., Weidner, G. A., Keller, L. M., Thom, J. E., & Cassano, J. J. (2012). Antarctic automatic weather station program: 30 years of polar observation. *Bull. Am. Meteorol. Soc.*, *93*, 1519–1537. doi:10.1175/BAMS-D-11-00015.1.

Le Vine, D. M., Lagerloef, G. S., & Torrusio, S. E. (2010). Aquarius and remote sensing of sea surface salinity from space. *Proc. IEEE*, *98*, 688–703. doi:10.1109/JPROC.2010.2040550.

Leduc-Leballeur, M., Picard, G., Mialon, A., Arnaud, L., Lefebvre, E., Possenti, P., & Kerr, Y. (2015). Modeling L-band brightness temperature at Dome C in Antarctica and comparison with SMOS observations. *IEEE Trans. Geosci. Remote Sens.*, *53*, 4022–4032. doi:10.1109/TGRS.2015.2388790.

Lemmetyinen, J., Schwank, M., Rautiainen, K., Kontu, A., Parkkinen, T., Mätzler, C., Wiesmann, A., Wegmüller, U., Derksen, C., Toose, P., Roy, A., & Pulliainena, J. (2016). Snow density and ground permittivity retrieved from L-band radiometry: Application to experimental data. *Remote Sens. Environ.*, *180*, 377–391. doi:10.1016/j.rse.2016.02.002.

Libois, Q., Picard, G., Arnaud, L., Dumont, M., Lafaysse, M., Morin, S., & Lefebvre, E. (2015). Summertime evolution of snow specific surface area close to the surface on the Antarctic Plateau. *The Cryosphere Discussions*, *9*, 2383–2398. doi:10.5194/tc-9-2383-2015.

Libois, Q., Picard, G., Arnaud, L., Morin, S., & Brun, E. (2014). Modeling the impact of snow drift on the decameter-scale variability of snow properties on the Antarctic Plateau. *J. Geophys. Res.-Atmos.*, *119*. doi:10.1002/2014JD022361.

Liu, H., Wang, L., & Jezek, K. C. (2006). Spatiotemporal variations of snowmelt in Antarctica derived from satellite scanning multichannel microwave radiometer and Special Sensor Microwave Imager data (1978–2004). *Journal of Geophysical Research: Earth Surface*, *111*. doi:10.1029/2005JF000318.

Long, D. G., & Drinkwater, M. R. (2000). Azimuth variation in microwave scatterometer and radiometer data over Antarctica. *IEEE Trans. Geosci. Remote Sens.*, *38*, 1857–1870. doi:10.1109/36.851769.

Macelloni, G., Brogioni, M., Pampaloni, P., Cagnati, A., & Drinkwater, M. R. (2006). DOMEX 2004: An experimental campaign at Dome-C Antarctica for the calibration of spaceborne low-frequency microwave radiometers. *IEEE Trans. Geosci. Remote Sens.*, *44*, 2642–2653. doi:10.1109/TGRS.2006.882801.

Macelloni, G., Brogioni, M., Pettinato, S., Zasso, R., Crepaz, A., Zaccaria, J., Padovan, B., & Drinkwater, M. (2013). Ground-based L-band emission measurements at dome-C Antarctica: The DOMEX-2 experiment. *IEEE Trans. Geosci. Remote Sens.*, *51*, 4718–4730. doi:10.1109/TGRS.2013.2277921.

Macelloni, G., Brogioni, M., & Rahmoune, R. (2012). Characterization of the spatial and temporal stability of the east-antarctic plateau in the low-microwave bands. *12th Specialist Meeting on Microwave Radiometry and Remote Sensing of the Environment (MicroRad)*, (pp. 1–4). doi:10.1109/MicroRad.2012.6185251.

Macelloni, G., Leduc-Leballeur, M., Brogioni, M., Ritz, C., & Picard, G. (2016). Analyzing and modeling the SMOS spatial variations in the East Antarctic Plateau. *Remote Sens. Environ.*, *180*, 193–204. doi:10.1016/j.rse.2016.02.037.

Mätzler, C. (1987). Applications of the interaction of microwaves with the natural snow cover. *Remote sens. rev.*, *2*, 259–387. doi:10.1080/02757258709532086.

Mätzler, C. (2006). *Thermal microwave radiation: applications for remote sensing* volume 52. Institution of Engineering and Technology.

McMullan, K., Brown, M. A., Martín-Neira, M., Rits, W., Ekholm, S., Marti, J., & Lemanczyk, J. (2008). SMOS: The payload. *IEEE Trans. Geosci. Remote Sens.*, *46*, 594–605. doi:10.1109/TGRS.2007.914809.

Mecklenburg, S., Drusch, M., Kerr, Y. H., Font, J., Martin-Neira, M., Delwart, S., Buenadicha, G., Reul, N., Daganzo-Eusebio, E., Oliva, R., & Crapolicchio, R. (2012). ESA's soil moisture and ocean salinity mission: Mission performance and operations. *IEEE Trans. Geosci. Remote Sens.*, *50*, 1354–1366. doi:10.1109/TGRS.2012.2187666.

Picard, G., Arnaud, L., Panel, J.-M., & Morin, S. (2016). Spatio-temporal evolution of snow depth observed by time-lapse laser scanning in the Alps and in Antarctica. *The Cryosphere Discussions*, . doi:10.5194/tc-2016-67.

Picard, G., Brucker, L., Roy, A., Dupont, F., Fily, M., Royer, A., & Harlow, C. (2013). Simulation of the microwave emission of multi-layered snowpacks using the Dense Media Radiative transfer theory: the DMRT-ML model. *Geosci. Model Dev.*, *6*, 1061–1078. doi:10.5194/gmd-6-1061-2013.

Picard, G., Domine, F., Krinner, G., Arnaud, L., & Lefebvre, E. (2012). Inhibition of the positive snow-albedo feedback by precipitation in interior Antarctica. *Nature Climate Change*, *2*, 795–798. doi:10.1038/nclimate1590.

Picard, G., Fily, M., & Gallée, H. (2007). Surface melting derived from microwave radiometers: a climatic indicator in Antarctica. *Ann. Glaciol.*, *46*, 29–34.

Picard, G., Royer, A., Arnaud, L., & Fily, M. (2014). Influence of meter-scale wind-formed features on the variability of the microwave brightness temperature around Dome C in Antarctica. *The Cryosphere*, *7*, 3675–3716. doi:doi:10.5194/tc-8-1105-2014.

Roy, A., Royer, A., Derksen, C., Langlois, A., & Sonnentag, O. (2016). Monitoring Boreal and Arctic Freeze/Thaw with the First Year of SMAP Brightness Temperatures. *IEEE Proc. of the 2016 14th Specialist Meeting on Microwave Radiometry and Remote Sensing of the Environment (MicroRad)*, .

Schneider, D. P., & Steig, E. J. (2002). Spatial and temporal variability of Antarctic ice sheet microwave brightness temperatures. *Geophysical Research Letters*, *29*. doi:10.1029/2002GL015490.

Shuman, C. A., & Alley, R. B. (1993). Spatial and temporal characterization of hoar formation in central Greenland using SSM/I brightness temperatures. *Geophys. Res. Lett.*, *20*, 2643–2646. doi:10.1029/93GL02810.

Skou, N., Kristensen, S. S., Søbjærg, S. S., & Balling, J. E. (2015). Airborne L-band radiometer mapping of the Dome-C area in Antarctica. *IEEE Journal of Selected Topics in Applied Earth Observations and Remote Sensing*, *8*, 3656–3664. doi:10.1109/JSTARS.2015.2425039.

Surdyk, S. (2002). Using microwave brightness temperature to detect short-term surface air temperature changes in Antarctica: An analytical approach. *Remote Sens. Environ.*, *80*, 256–271. doi:10.1016/S0034-4257(01)00308-X.

Tan, S., Aksoy, M., Brogioni, M., Macelloni, G., Durand, M., Jezek, K. C., Wang, T.-L., Tsang, L., Johnson, J. T., Drinkwater, M. R., & Brucker, L. (2015). Physical Models of Layered Polar Firn Brightness Temperatures From 0.5 to 2 GHz. *IEEE Journal of Selected Topics in Applied Earth Observations and Remote Sensing*, *8*, 3681–3691. doi:10.1109/JSTARS.2015.2403286.

Tedesco, M., & Monaghan, A. J. (2009). An updated Antarctic melt record through 2009 and its linkages to high-latitude and tropical climate variability. *Geophys. Res. Lett.*, *36*. doi:10.1029/2009GL039186.

Tiuri, M., Sihvola, A., Nyfors, E., & Hallikaiken, M. (1984). The complex dielectric constant of snow at microwave frequencies. *IEEE J. Ocean. Eng.*, *9*, 377–382. doi:10.1109/JOE.1984.1145645.

Torinesi, O., Fily, M., & Genthon, C. (2003). Variability and trends of the summer melt period of Antarctic ice margins since 1980 from microwave sensors. *Journal of Climate*, *16*, 1047–1060.

Tsang, L., Kong, J. A., & Ding, K.-H. (2000). *Scattering of Electromagnetic Waves, vol.1: Theories and Applications*. Wiley Interscience.

Vaughan, D. G., Bamber, J. L., Giovinetto, M., Russell, J., & Cooper, A. P. R. (1999). Reassessment of net surface mass balance in Antarctica. *Journal of climate*, *12*, 933–946.

West, R. D., Winebrenner, D. P., Tsang, L., & Rott, H. (1996). Microwave emission from density-stratified Antarctic firn at 6 cm wavelength. *J. Glaciol.*, *42*, 63–76.

Wiesmann, A., & Mätzler, C. (1999). Microwave emission model of layered snowpacks. *Remote Sens. Environ.*, *70*, 307–316. doi:10.1016/S0034-4257(99)00046-2.

Winebrenner, D. P., Steig, E. J., & Schneider, D. P. (2004). Temporal co-variation of surface and microwave brightness temperatures in Antarctica, with implications for the observation of surface temperature variability using satellite data. *Ann. Glaciol.*, *39*, 346–350. doi:10.3189/172756404781813952.

Zwally, J. H. (1977). Microwave emissivity and accumulation rate of polar firn. *J. Glaciol.*, *18*, 195–215. doi:10.3198/1977JoG18-79-195-215.